arXiv:0710.4003v1 [astro-ph] 22 Oct 2007

P. Demarque, D. B. Guenther, L. H. Li, A. Mazumdar and C. W. Straka

YREC: The Yale Rotating Stellar Evolution Code

Non-rotating version, seismology applications

Abstract The stellar evolution code YREC is outlined with emphasis on its applications to helio- and asteroseismology. The procedure for calculating calibrated solar and stellar models is described. Other features of the code such as a non-local treatment of convective core overshoot, and the implementation of a parametrized description of turbulence in stellar models, are considered in some detail. The code has been extensively used for other astrophysical applications, some of which are briefly mentioned at the end of the paper.

Keywords methods: numerical · stars: evolution · stars: interior · convection

PACS 97.10.Cv · 96.60.Ly · 92.60.hk

1 Introduction

The aim of this paper is to provide an overview of the Yale Rotating Stellar Evolution Code (YREC), as it has been applied in the last few years to research in helio- and asteroseismology. Although YREC contains extensions to model the effects of rotation in an oblate coordinate system, we describe here the "non-rotating" version.

P. Demarque, L. H. Li, A. Mazumdar
Department of Astronomy, Yale University,
New Haven, CT 06520-8101, USA
E-mail: pierre.demarque@yale.edu
E-mail: li@astro.yale.edu
E-mail: anwesh.mazumdar@yale.edu

D. B. Guenther
Department of Astronomy and Physics,
Institute for Computational Astrophysics,
Saint Mary's University,
Halifax, Nova Scotia, Canada B3H 3C3
E-mail: guenther@ap.smu.ca

C. W. Straka
Centro de Astrofísica da Universidade do Porto (CAUP),
Rua das Estrelas, 4150-762 Porto, Portugal
E-mail: straka@astro.up.pt

In addition to a general description, we shall emphasize three features of the code which have been implemented because of their special relevance to seismology. The first feature is the procedure utilized for the automatic calculation of calibrated solar and stellar models whose pulsational properties are to be investigated. The second feature is the treatment of convective core overshoot. Finally, the third feature is the implementation in stellar models of the effects of turbulence on the structure of the surface layers of stars with a convective envelope. The parametrization of turbulence to one dimension is based on three-dimensional radiative hydrodynamical (3D HRD) simulations of the highly superadiabatic layer (SAL) in the atmosphere. The interaction of turbulent convection and radiation in these thin transition regions is poorly known. Oscillation frequencies are sensitively affected by the structure of transition regions between radiative and convective layers. Seismology thus offers a unique opportunity to explore a long standing problem in stellar physics.

Like most stellar evolution codes, YREC is a continuously evolving research tool to which many have contributed. As a result, different versions of YREC are in use at several institutions, which have been applied to a variety of research purposes. Some of the most significant applications of YREC are listed in the text and at the end of this paper (see Sect. 13). The rotating version of YREC, originally developed by Pinsonneault (1988), includes a 1.5D treatment of rotation, extending the work of Kippenhahn & Thomas (1970) and Endal & Sofia (1981), and using the formalism of Law (1980). A 2D version of YREC has also recently been implemented, specifically to address some fundamental aspects of solar magnetic activity (Li et al. 2006).

Sect. 2 outlines the numerical scheme adopted to solve the classical differential equations of stellar structure and evolution. The treatment of the boundary conditions, of special importance for seismology, are described in Sect. 3. The constitutive physics, i.e. the equation of state and radiative and conductive opacities, are reviewed in Sect. 4, and the nuclear processes are described in Sect. 6. Stellar physics topics such as superadiabatic convection, element diffusion, convective core overshoot, and turbulence in the outer lay-

ers, all of which also have important seismological signatures, are covered in Sect. 3.2, Sect. 5, Sect. 9 and Sect. 10, respectively. The operation of the code is described in Sect. 7, with emphasis on helio- and asteroseismic applications. Seismic diagnostics applications are described in Sect. 11. The role played by YREC in the research on solar neutrinos and helio-seismology is summarized in Sect. 12. Studies of advanced evolutionary phases and applications to stellar population studies are listed in Sect. 13.

2 Henyey code

The four first-order simultaneous equations of stellar structure are well-known, and have been frequently discussed in the literature (Schwarzschild 1958). YREC uses mass as the independent variable in the formulation of the equations (Lagrangian formulation). The problem is a two-point boundary value problem, with boundary conditions at the center and at the surface of the model. A relaxation technique, based on a finite difference approximation, is used. The method, first applied to the stellar structure problem by Henyey et al. (1959), is known as the Henyey method. Useful descriptions of the Henyey method are given in the paper by Larson & Demarque (1964) and the book by Kippenhahn & Weigert (1990). Specific details about the numerical procedures in the YREC implementation can be found in the Appendices of Prather (1976), which describe an earlier Henyey code on which YREC is based. Prather (1976) also provides information about the treatment of the constitutive physics, although most of the physics details have been updated since then.

In the Henyey method, the model star is divided into n concentric shells by means of $n + 1$ suitably chosen values of the independent variable (mass), or points, in the interval defined by the innermost point (near the center) and the outermost point, which is specified by the user and located at the base of the envelope integrations. The four differential equations are replaced in each shell by approximating difference equations relating the values of the dependent variables at adjacent points. There are four dependent variables in each of the n shells, providing a set of $4(n + 1)$ linear equations which, together with two boundary conditions at the center and two at the surface, can be solved to determine approximate corrections to the $4(n + 1)$ dependent variables, starting from a first approximation model. The set of simultaneous equation is solved by iteration until the corrections in each variable satisfy a specified convergence limit.

2.1 Shell redistribution

The shells are distributed so as to optimize numerical accuracy and efficiency. In order to follow the evolution from the earliest gravitational contraction phase all the way to the hydrogen and helium shell burning phases, it is necessary to redistribute the shells in the model. This is especially critical during shell burning. After a star exhausts its core supply

of hydrogen it begins burning hydrogen in a shell. Initially the shell is almost $0.2M_\odot$ thick for a $1M_\odot$ star but the shell quickly narrows to only $0.001M_\odot$ as the star evolves up the giant branch, thinning to $0.0001M_\odot$ at the point of helium flash. Because of the high temperature dependence of helium burning, helium burning shells are even thinner than hydrogen burning shells. YREC will add or remove shells according to the size of gradients in structure (i.e., pressure, temperature, and composition) and gradients in luminosity, as well as the size of Henyey corrections applied during the iteration procedure. The code keeps track of physically real discontinuities so that they are not smoothed during the rezoning process. Interpolation is linear. Our own testing has shown that using higher order methods such as oscillatory spline interpolation introduces numerical oscillations near the tip of the giant branch.

2.2 Time steps

The models are advanced in time through two terms in the energy equation, the nuclear energy term (Sect. 6), and the time rate of change of entropy due to contraction or expansion during evolution. Special care is taken to preserve numerical accuracy for small time steps (Prather (1976)).

One can either specify the time step or have YREC automatically determine the optimum time step during evolution. When producing accurately calibrated solar models, to maintain numerical consistency it helps to specify the time step interval. In most other situations it is best to let YREC determine the time step based on user specified convergence tolerance criteria. During nuclear burning phases of evolution YREC will guess the time step based on the rate at which hydrogen and helium (if applicable), are being consumed in each shell of the model. During gravitational contraction phases of evolution YREC will control the time steps by monitoring the change in temperature, pressure, and luminosity from one model to the next. During helium flash if the model fails to converge during a evolutionary time step, YREC is also able reduce the time step by a user specified factor and redo the evolutionary step. More details regarding the operation of YREC can be found in Sect. 7.

3 Boundary conditions

3.1 Center

The two inner boundary conditions constrain the values of the radial distance and luminosity variables at the innermost mass shell. Because of the false singularity at the center, the innermost point is not at the very center, but in a shell chosen close to the center. Note that in order to preserve accuracy, special care must be taken with the position of the innermost shell, especially in pulsation calculations (see Sect. 7.3).

3.2 Surface

The outer boundary conditions depend on the structure near the surface. Because a model of the outer layers depends on the global properties of the star, i.e. its surface gravity log g and effective temperature T_{eff}, the problem is implicit. In order to specify the surface boundary conditions, which relate the variations of the pressure and temperature variables to the total luminosity and radius of the star, three inward envelope integrations are constructed. These envelope integrations are chosen so as to form a triangle in the theoretical HR-diagram (i.e. the log $L/L_\odot$ vs. log T_{eff} plane).

The inward envelope integrations consist of two main parts. The outermost layers, starting at optical depth near $\tau = 10^{-10}$, which are effectively isothermal at the start, are described by a gray radiative atmosphere specified by a $T(\tau)$ relation and integrated to the appropriate value of τ at which the temperature reaches T_{eff} (e.g. $\tau = 2/3$ for the Eddington approximation, $\tau = 0.312156330$ for the Krishna Swamy (1966) atmosphere). This surface in the star is usually defined as the *photosphere*.

As an alternative to the atmosphere integrations, more complex atmospheres from pre-computed libraries can be also used, such as those from Kurucz (1998).

Below the photosphere, all variables but the luminosity variable (which is held to be constant in the outer envelope) are integrated to a chosen value of the mass. The integration is carried out using log P as the independent variable, to the value of the mass variable at which the surface boundary conditions for the interior are computed (the base of the envelope). The region which extends from this value of the mass to the innermost shell of the star constitutes the *interior* of the stellar model. In convectively unstable layers of the envelope (as determined by the local Schwarzschild criterion), the temperature gradient is evaluated according to the formalism of Stothers & Chin (1995), which is designed to describe superadiabatic convection. It is in this region that the peak of the highly superadiabatic transition layer (SAL) is normally located (as it is in the Sun). The main advantage of the Stothers & Chin (1995) formalism is that by a suitable choice of parameters, it can be made to reproduce either the standard *mixing length theory* (MLT) (Böhm-Vitense 1958) or the theory of Canuto & Mazzitelli (1992), sometimes called FST. In order to preserve continuity in the convective temperature gradient at the envelope-interior interface, the Stothers & Chin (1995) formalism is used to calculate the convective gradient both in the envelope and in the interior whenever superadiabaticity exceeds a preset value.

Another feature of the envelope integration, described in more detail in Sect. 10, includes a 1D parametrization of the effects of turbulent pressure and turbulent kinetic energy in the outer layers.

4 Equation of state and opacities

YREC has been updated regularly so as to incorporate the latest research developments regarding equation of state and opacity in the stellar interior, while maintaining backward compatibility with earlier versions of the same. The current version uses the latest OPAL opacities (Iglesias & Rogers 1996) and OPAL equation of state (Rogers & Nayfonov 2002). At low temperatures (log $T < 4.1$) opacities are obtained from the tables provided by Ferguson et al. (2005).
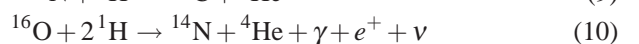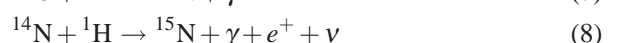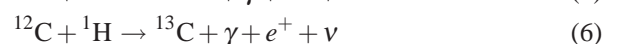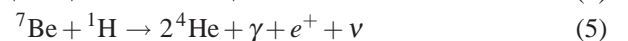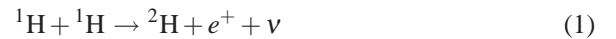
At each mass shell the EOS is obtained by interpolation from the standard tables. Since the EOS is weakly dependent on Z, we use only one set of tables at a fixed Z, obtained by the Z-interpolation routine provided with the OPAL EOS package. For models with metal diffusion, the value of Z at which the EOS is interpolated is chosen at a suitable intermediate value. The EOS quantities at the desired X, T and ρ are obtained by quadratic interpolation from the tables. The results and the derivatives are smoothed by mixing overlapping quadratics. For opacity, a four-point Lagrangian interpolation scheme is used over a 4-dimensional grid of Z, X, T, and ρ.

5 Diffusion

The diffusion of chemical elements by gravitational settling and thermal diffusion is implemented following the prescription of Thoul et al. (1994). Options in the code include no diffusion, helium diffusion only, or both Y and Z diffusion. The analytical fits provided by Thoul et al. (1994) can also be used instead of the tabulated diffusion coefficients, to speed up the computations.

6 Nuclear Reactions

The nuclear reaction rates in conjunction with the corresponding energy release (Q-values) are important for the evolution of chemical species, the energy input from nuclear fusion reactions and for the neutrino fluxes. The reactions explicitly calculated in YREC are the following:

$$^1\mathrm{H} + {}^1\mathrm{H} \to {}^2\mathrm{H} + e^+ + \nu \tag{1}$$

$$^3\mathrm{He} + {}^3\mathrm{He} \to {}^4\mathrm{He} + 2\,{}^1\mathrm{H} \tag{2}$$

$$^3\mathrm{He} + {}^4\mathrm{He} \to {}^7\mathrm{Be} + \gamma \tag{3}$$

$$^7\mathrm{Be} + e^- + {}^1\mathrm{H} \to 2\,{}^4\mathrm{He} + \nu \tag{4}$$

$$^7\mathrm{Be} + {}^1\mathrm{H} \to 2\,{}^4\mathrm{He} + \gamma + e^+ + \nu \tag{5}$$

$$^{12}\mathrm{C} + {}^1\mathrm{H} \to {}^{13}\mathrm{C} + \gamma + e^+ + \nu \tag{6}$$

$$^{13}\mathrm{C} + {}^1\mathrm{H} \to {}^{14}\mathrm{N} + \gamma \tag{7}$$

$$^{14}\mathrm{N} + {}^1\mathrm{H} \to {}^{15}\mathrm{N} + \gamma + e^+ + \nu \tag{8}$$

$$^{15}\mathrm{N} + {}^1\mathrm{H} \to {}^{12}\mathrm{C} + {}^4\mathrm{He} \tag{9}$$

$$^{16}\mathrm{O} + 2\,{}^1\mathrm{H} \to {}^{14}\mathrm{N} + {}^4\mathrm{He} + \gamma + e^+ + \nu \tag{10}$$

$$3\,{}^4\mathrm{He} \to {}^{12}\mathrm{C} \tag{11}$$

$$^{12}\text{C} + {}^{4}\text{He} \rightarrow {}^{16}\text{O} + \gamma \tag{12}$$

$$^{13}\text{C} + {}^{4}\text{He} \rightarrow {}^{16}\text{O} + \text{n} \tag{13}$$

$$^{14}\text{N} + {}^{4}\text{He} \rightarrow {}^{18}\text{O} + \gamma \tag{14}$$

$$2\,{}^{1}\text{H} + e^{-} \rightarrow {}^{2}\text{H} + \nu \tag{15}$$

$$^{3}\text{He} + {}^{1}\text{H} \rightarrow {}^{4}\text{He} + e^{+} + \nu \tag{16}$$

The first five Equations (1-5) contain the three alternative pp branches ($pp1, pp2, pp3$) all of which start with ^{3}He. Equations (6)-(9) represent the primary CNO cycle, (10) the secondary cycle. The reaction of helium burning is given in Equation (11), followed by the dominant α capture reactions (12)-(14). The last two reactions are only important for the neutrino problem and can be neglected for the energy generation. As is implicitly shown in the nuclear reactions (1-16), all β-decay reactions are treated in the instantaneous approximation. In addition, four branching ratios are defined (Bahcall & Ulrich 1988): the fraction of ^{7}Be that is burned by electron capture (4), the fraction of ^{7}Be that is burned by proton capture (5), the fraction of ^{14}N that is burned via $^{14}\text{N}(\text{p},\alpha)^{12}\text{C}$ and the fraction of ^{15}N that is burned via $^{15}\text{N}(\text{p},\gamma)^{16}\text{O}$.

The energy generation is calculated by multiplying the rates by the Q-values which are taken from Bahcall & Ulrich (1988, Table 21). The standard reaction rates implemented are identical to the rates published in Bahcall (1989).

6.1 NACRE

YREC provides the option of using the NACRE[1] reaction rates (Angulo et al. 1999). In its present version, the Q-values from each reaction are *not* changed and are thus not identical to the values published on the NACRE database[2]. All relevant reaction rates that are provided by NACRE are included, i.e. those corresponding to Equations (1-3; 5-11).

The NACRE library lists the rate data in tabulated form and also provides fit-formulas, the latter of which are implemented. The fit-formulas are accurate by 3% - 25% compared to the tabulated data, with typical deviations of 10% - 15%.

Our tests for a standard solar model have shown that a calibrated standard model is not affected by the NACRE reaction rates. The largest differences are found in the neutrino flux of ^{8}B which differs by about 9%. This difference is comfortably within other theoretical uncertainties (Bahcall et al. 2004).

6.2 Light elements

A switch permits keeping track of nuclear burning of the light elements ^{2}H, ^{6}Li, ^{7}Li and ^{9}Be at the base of the convection zone in models of sun-like stars (Deliyannis 1990).

[1] Nuclear Astrophysics Compilation of REaction Rates
[2] http://pntpm.ulb.ac.be/Nacre

6.3 Neutrino losses

Neutrino loss rates are taken from the monograph by Bahcall (1989), updated by subsequent private communications from the author. For advanced stages of stellar evolution, the neutrino rates from photo, pair and plasma sources from Itoh et al. (1989) are included.

7 Running YREC

YREC can automatically calculate calibrated solar and stellar models. The user provides a complete set of constraints along with allowable parameter variations and YREC will search within the chosen parameter space for a solution. This is especially convenient since the mixing length parameter and in some cases the helium abundance used to compute stellar models must first be established from calibrated solar models. The calibrated values are sensitive to the choice of opacity tables, the equation of state formulation, the inclusion of diffusion, and the choice of model atmosphere.

7.1 Calibrated solar models

To produce a calibrated solar model the user inputs the age of the Sun and its primordial composition, i.e., mass fraction mixture of hydrogen, helium, and metals on the zero age main-sequence. In addition the user specifies the tolerances for the luminosity and radius. YREC will then vary the initial value for the helium abundance and mixing length parameter until it has produced a model at the age of the Sun that has the observed radius, 6.958×10^{10} cm, and observed luminosity, 3.8515×10^{33} erg/s (Edmonds et al. 1992) within the specified tolerances. When including the effects of metal and helium diffusion, the user has the option of inputting the Z/X at the surface and its allowed tolerance. In this case, YREC will adjust the initial helium abundance, metal abundance, and mixing length until a model at the age of the Sun is produced that matches the Sun's luminosity, radius, and surface Z/X within the specified tolerances. With 64-bit floating point numbers, YREC can compute a tuned solar model with tolerances of 1 part in 10^{6} for radius and luminosity and 1 part in 10^{4} in Z/X after about 10 to 12 iterations.

The actual procedure begins by computing one reference run, one run with slightly changed helium abundance, followed by one run with slightly changed mixing length parameter, and then one run, if chosen, with slightly changed metal abundance. The luminosity, radius, and, if chosen, surface Z/X, of the final models are used to compute the derivative matrix of luminosity, radius and surface Z/X with respect to helium abundance, mixing length parameter, and Z. The first order corrections to each parameter are determined from the derivative matrix and a new model is computed. The process is iterated until the model falls within the specified tolerances.

7.2 Calibrated stellar models

The process is slightly different for stars because normally the age of a star is unknown. Only the luminosity and surface temperature are used to constrain the model. In the case of stars, YREC adjusts the mass and either the mixing length parameter or the helium abundance in an attempt to produce a stellar evolutionary track that passes though the tolerance box in the theoretical HR-diagram.

To produce a stellar model the user inputs the metal abundance, and either the helium abundance or the mixing length parameter. In addition the user specifies the luminosity, effective temperature, and their corresponding tolerances. The user has the option of allowing the code to adjust either the mixing length parameter or the helium abundance. The code generates tracks varying the mass and the chosen parameter using a derivative matrix to produce a model that passes through the specified location in the HR-diagram. Once the optimum parameters are determined, the code computes the track a second time but stops the evolution when the model hits the specified location in the HR-diagram. The tuned model is constrained in mass and age.

7.3 Pulsation models

The pulsation output files in YREC are tailored for the JIG non-adiabatic oscillation code of Guenther (Guenther 1994). These files can be saved for specified models in an evolutionary sequence (say for a calibrated solar model, or for a calibrated stellar model), or any model for specified ages along the evolutionary track.

One of the first things stellar modelers realized when using their solar models for pulsation analysis is that the optimum distribution of shells within the model for structure and evolutionary calculations is different from the optimum distribution of shells for pulsation analysis. Whereas evolutionary models need to resolve well the nuclear burning regions, pulsation models need to resolve the surface layers (for acoustic modes). For example, for evolutionary models great care is needed to fully resolve the thinning hydrogen burning shell ($0.001\,M_\odot$ to $0.0001\,M_\odot$) as the models evolve up the giant branch. For pulsation models it is the low density regions, where the sound waves have the largest amplitudes, that need to be well resolved. Therefore, in order to produce viable models for pulsation analysis, the user increases the resolution of shells in the envelope, atmosphere, and the region below the base of the convection zone. Ultimately, in order to achieve frequency accuracies of the order of 1 part in 10^4 using a first order numerical pulsation program one needs approximately 600 shells in the interior, 600 shells in the envelope defined as the outer $1-5\%$ of the mass, and 600 shells in the atmosphere. To maximize self consistency all thermodynamic variables and their derivatives are obtained directly from the structure model.

Related to shell resolution is the distribution of shells near the core. Stellar evolutionary codes do not locate a shell at the center owing to divide by zero complications but set the innermost shell a small distance away from the center. In order to do accurate pulsation analysis of g-modes or to study the p-mode small spacing parameter, both of which are sensitive to the structure of the deep interior, it is necessary to extend the innermost shell closer to the center than normally required by stellar evolutionary calculations: compare 1.0×10^{-3} radius fraction for stellar evolution to 2.0×10^{-7} for stellar pulsation. A stellar model output for pulsation runs from the "central-most" interior shell to the top of atmosphere computation near optical depth $\tau = 10^{-10}$.

7.4 Model grids

A useful feature of YREC is its ability to carry out extensive model calculations without user input. It is possible to generate in a single run, tens of thousands of evolutionary tracks, corresponding to tens of millions of models, covering a wide range of masses, compositions, mixing length parameters, with each track tuned to their own particular numerical and physical variables. This has enabled Guenther & Brown (2004) to compute dense grids of stellar models for pulsation analysis throughout the HR-diagram. For other grids of evolutionary sequences, see Sect. 13.

7.5 Backwards compatibility

All new physics (e.g., opacities, nuclear reaction rates) have been implemented along with existing physics so that the user can, at any time, run YREC using older physics.

8 Convection

By default the local Schwarzschild criterion is implemented in order to determine if a mass shell is labeled as *convective* or *radiative*. The Ledoux stability criterion can also be used when a specific parameter choice is made in the local limit of the non-local convection treatment described below. The abundance of chemical species in convective cores is treated under the assumption of instantaneous mixing.

9 Core Overshoot

Since the eddy velocity at convective boundaries is non-zero, convective motions will penetrate into the radiative region. Two different forms of penetration are commonly distinguished: (a) inefficient penetration that does not alter the temperature gradient, termed "overmixing" here, and (b) subadiabatic penetration (Zahn 1991), where the convective heat transport is efficient enough to establish a nearly adiabatic temperature gradient.

YREC offers a number of different options for treating overshoot (OS). All OS options have in common that mixing

of chemical species in the OS region is instantaneous and all chemical species are homogenized within the extended zone. Due to the small characteristic time scale of convection in comparison to the thermal and nuclear timescales during the major burning stages this assumption holds to high accuracy.

Among the OS options, two different approaches are distinguished: (a) a parametric treatment where the OS extent is a multiple of the pressure scale height taken at the formal Schwarzschild boundary and (b) a physically motivated treatment where the OS extent is calculated from a non-local convection theory originally developed by Kuhfuß (1986) and later extended by Wuchterl & Feuchtinger (1998). In the latter case, the temperature gradient is calculated directly from the additional convection equation which is solved in addition to the canonical stellar structure equations at every time-step.

9.1 Parametric Treatment

The boundary of the OS zone is determined by adding a fraction α_{OM} of the pressure scale height to the boundary at the radius r_S, determined by the Schwarzschild criterion:

$$r_{new} = r_S + \alpha_{OM} H_P(r_S) \qquad (17)$$

where the pressure scale height $H_P(r_S)$ is taken at the Schwarzschild boundary. The temperature stratification in the OS zone is determined by the two options described above, either (a) the temperature gradient is not altered (overmixing) or (b) the temperature gradient is set to the adiabatic temperature gradient. For a fixed α_{OM} the latter option produces larger convective cores (Zahn 1991).

9.2 Non-local Convection

As an alternative to the purely parametric treatment of OS, the one-dimensional convection theory developed by Kuhfuß (1986) is implemented (Straka et al. 2005). In the framework of anelastic and diffusion-type approximations of the unknown correlation functions, Kuhfuß derives one equation for the turbulent kinetic energy from spherical averages of the first-order perturbed Navier-Stokes equations. The solution of this equation provides the extent of the convective core region and includes the effects of OS naturally, since the velocity of convective motions is zero where the turbulent kinetic energy vanishes. In addition, this equation also provides the temperature gradient in the OS region.

9.2.1 Implemented Equations

The new equation for the turbulent kinetic energy $\bar{\omega}$ that is solved in YREC is given by:

$$\frac{D\bar{\omega}}{Dt} = \frac{\nabla_{ad}}{\rho H_P} j_{\bar{\omega}} - \frac{c_D}{\Lambda} \bar{\omega}^{3/2} - \frac{\partial}{\partial m}\left(4\pi r^2 j_t\right), \qquad (18)$$

$$j_t = -4\pi r^2 \rho^2 \alpha_t \Lambda \bar{\omega}^{1/2} \frac{\partial \bar{\omega}}{\partial m} \qquad (19)$$

Table 1 Parameters of non-local convection theory

parameter	canonical value	description
α_{MLT}	1.5	mixing length
α_s	0.408	turbulent driving
c_D	2.177	dissipation efficiency
α_t	$0.610\,\alpha_s$	overshoot distance
β_r	1.0	geometric mixing length

where D/Dt is the Lagrangian time derivative, ρ density, r stellar radius, m the Lagrangian mass coordinate. Λ, defined as $1/\Lambda = 1/(\alpha_{MLT}H_P) + 1/(\beta_r r)$ is the geometrically limited mixing length scale with ∇_{ad} being the adiabatic gradient. Note that the limiting of the pressure scale height in the central part influences the total core size within the framework of non-local convection theories.

A linear implicit extrapolation method is used in order to calculate the stationary solution of Equation (18), i.e. $D\bar{\omega}/Dt \equiv 0$. The solution yields the turbulent kinetic energy $\bar{\omega}$ at every mass shell. We define shells to be convective, if:

$$x_{\bar{\omega}} < 0.1 \qquad (20)$$

where

$$x_{\bar{\omega}} = \frac{1}{1 + F\,\bar{\omega}^{1/2}}, \qquad F = \frac{3\alpha_s\,\kappa\rho^2\,\Lambda C_P}{16\sigma T^3} \qquad (21)$$

with the usual notation for the opacity κ, temperature T, specific heat at constant pressure C_P and the Stefan-Boltzmann constant σ. The boundaries are sharply defined by an extreme falloff of $\bar{\omega}$ which is encountered in interior solutions of Equation (18). Finally, the temperature gradient can be calculated from:

$$\nabla = \nabla_{ad} + x_{\bar{\omega}}\left(\nabla_{rad} - \nabla_{ad}\right) + (1 - x_{\bar{\omega}})\left(G\frac{\partial\bar{\omega}}{\partial n} + H\right) \qquad (22)$$

with

$$G = \frac{\alpha_t}{\alpha_s}\frac{H_P}{C_P T}\left(\frac{4\pi r^2\rho}{\Delta m}\right), \qquad (23)$$

$$H = \frac{\varphi}{\delta}\nabla_\mu \qquad (24)$$

where Δm is the mass enclosed in one shell and $\nabla_\mu = d\ln\mu/d\ln P$. In the case of an ideal gas with radiation pressure the dimensionless parameters δ and φ take on the values $\delta = (4 - 3\beta)/\beta$, $\beta = P_{gas}/P$ and $\varphi = 1$ respectively. In convective core regions, the temperature gradient remains very close to the adiabatic one whenever $x_{\bar{\omega}} < 0.1$. A more detailed discussion of the implemented equations and the numerical techniques employed can be found in Straka et al. (2005).

9.2.2 Non-local parameters

The implemented non-local convection theory contains five parameters (Table 1). These parameters must be calibrated, preferably on a well selected set of open clusters, or on selected asteroseismic target stars like Procyon A (Straka et al.

2005). Two of the canonical values given in Table 1, i.e. α_s and α_t can be derived by matching the Kuhfuß result to *mixing length theory* (MLT) in the local limit ($\alpha_t = 0$).

The mixing-length parameter plays a minor role in the core regions, where superadiabaticity of temperature gradient is tiny. The parameter that controls the OS zone is given by α_t and is thus the most important one to calibrate. Kuhfuß derives $\alpha_t = 0.610\,\alpha_s$ from theoretical arguments.

In the strictly local limit ($\alpha_t = 0$) the Kuhfuß treatment is equivalent to the MLT equations when based on the Ledoux stability criterion.

10 Turbulence

A method to incorporate the effects of turbulence into the outer layers of one-dimensional (1D) stellar models has been implemented in YREC (Li et al. 2002). The method requires a detailed three-dimensional hydrodynamical simulation (3D RHD) of the atmosphere and highly superadiabatic layer of stars (Robinson et al. 2003).

The basic idea is to extract from the velocity field of the 3D simulation three important quantities: the turbulent pressure, the turbulent kinetic energy and the anisotropy of the flow. Implementation into a 1D stellar model thus requires two additional parameters, i.e. χ, the specific turbulent kinetic energy, and γ, which reflects the flow anisotropy. These parameters, which modify the hydrostatic equilibrium equation and the internal energy equation, must be introduced in a thermodynamically self-consistent way. As a result, they also change the adiabatic and convective temperature gradients, as well as the energy conservation equation.

The next section (Sect. 10.1) describes the calculation of χ and γ from the velocity field in the 3D simulation. The introduction of the parameters χ and γ into the stellar structure equations and YREC is summarized in Sect. 10.2, Sect. 10.3 and Sect. 10.4. The effects on p-mode frequencies in a solar model are illustrated in Sect. 10.5.

10.1 Turbulent velocities

The physics (thermodynamics, the equation of state, and opacities) in the 3D simulation is the same as in the 1D stellar models. These simulations follow closely the approach described by Kim & Chan (1998), and are described in more detail in the papers of Robinson et al. (2003, 2004). The full hydrodynamical equations were solved in a thin subsection of the stellar model, i.e. a 3D box located in the vicinity of the photosphere. For the radiative transport, the diffusion approximation was used in the deep region ($\tau > 10^3$) of the simulation, while the 3D Eddington approximation was used (Unno & Spiegel 1966) in the region above. After the simulation had reached a steady state, statistical integrations were performed for each simulation for over 2500 seconds in the case of the solar surface convection.

For the derivation of χ and γ, Li et al. (2002) use a self-consistent approach introduced by Lydon & Sofia (1995) to include magnetic fields in calculating the convective temperature gradient within the MLT framework, and used successfully by Lydon et al. (1996) to explain the variation of solar p-modes with the solar cycle.

Turbulence can be measured by the turbulent Mach number $\mathcal{M} = v''/v_s$, where v'' is the turbulent velocity, and v_s is the sound speed. The MLT is valid when $\mathcal{M}$ is sufficiently small. In the outer layers of a star like the sun $\mathcal{M}$ can be of order unity (Cox & Giuli 1968), but in the deep convection region $\mathcal{M}$ is almost zero. The turbulent velocity is defined by the velocity variance:

$$v''_i = (\overline{v_i^2} - \overline{v_i}^2)^{1/2}, \tag{25}$$

where the overbar denotes a combined horizontal and temporal average, and v_i is the total velocity.

Using $\mathcal{M}$, we can define the turbulent kinetic energy per unit mass χ as

$$\chi = \frac{1}{2}\mathcal{M}^2 v_s^2. \tag{26}$$

The turbulent contribution to the entropy is

$$S_{\text{turb}} = \chi/T, \tag{27}$$

where T is the gas temperature.

Turbulence in the stratified layers of a stellar convection zone is not isotropic. We define the parameter γ to reflect the anisotropy of turbulence,

$$P_{\text{turb}} = (\gamma - 1)\rho\chi, \tag{28}$$

where $\rho\chi$ is the turbulent kinetic energy density. Since $P_{\text{turb}} = \rho v''^2_z$, γ can be related to the turbulent velocity as follows:

$$\gamma = 1 + 2(v''_z/v'')^2. \tag{29}$$

$\gamma = 5/3$ when turbulence is isotropic ($v''_z = v''_x = v''_y$); $\gamma = 3$ or $\gamma = 1$ when turbulence is completely anisotropic ($v''_z = v''$ or $v''_z = 0$, respectively). The physical meaning of γ is the specific heat ratio due to turbulence. This affects the distribution of the radial turbulent pressure which is then scaled with the gas pressure, P_{gas}. The total pressure is defined as

$$P_T = P_{\text{gas}} + P_{\text{rad}} + P_{\text{turb}}. \tag{30}$$

10.2 Convective temperature gradients with the turbulent velocities

Since the parameters χ and γ now appear in the equation of state, they must be included as independent variables in evaluating the density derivative. We have therefore:

$$d\rho/\rho = \mu\, dP_T/P_T - \mu'\, dT/T - \nu\, d\chi/\chi - \nu'\, d\gamma/\gamma, \tag{31}$$

where

$$\mu = \left(\frac{\partial \ln\rho}{\partial \ln P_T}\right)_{T,\chi,\gamma} \quad \mu' = -\left(\frac{\partial \ln\rho}{\partial \ln T}\right)_{P_T,\chi,\gamma}$$

$$\nu = -\left(\frac{\partial \ln\rho}{\partial \ln\chi}\right)_{P_T,T,\gamma} \quad \nu' = -\left(\frac{\partial \ln\rho}{\partial \ln\gamma}\right)_{P_T,T,\chi}$$

As a result, the stability criterion against convection is modified. For similar reasons, both the convective and adiabatic gradients are also modified by turbulence.
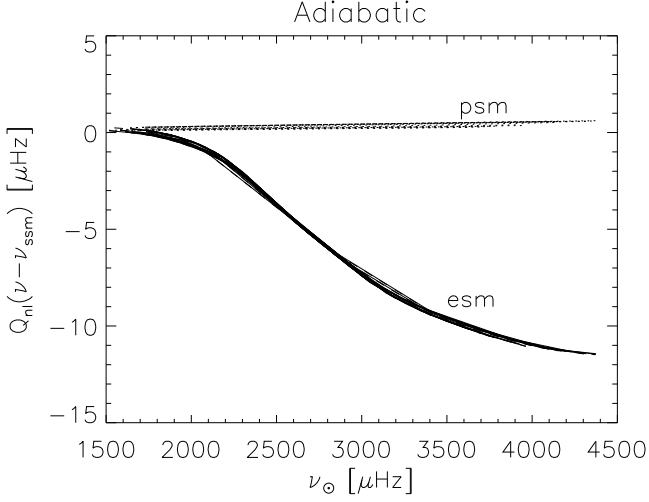
Fig. 1 *P*-mode frequency difference diagrams. Turbulent model minus standard model (ssm), for the turbulent pressure solar model (psm), and the solar model with the turbulent pressure and turbulent kinetic energy (esm). The difference between psm and ssm is of the order of 1μ Hz, while at high frequencies esm and ssm differ by more than 10 μ Hz. Plotted are the $l = 0, 1, 2, 3, 4, 10, 20, \ldots, 100$ *p*-modes.
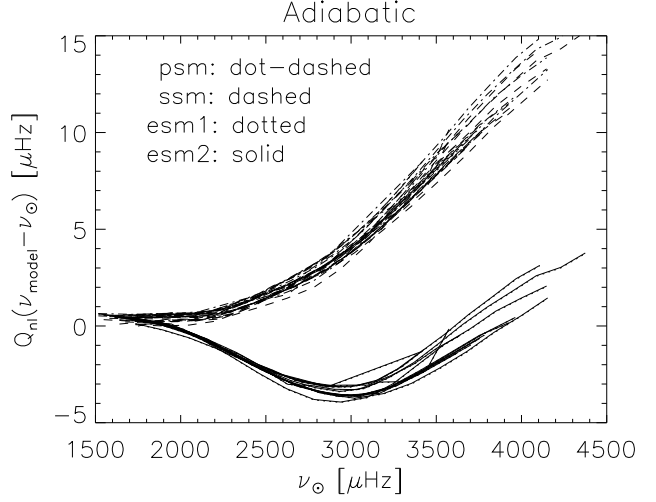
Fig. 2 *P*-mode frequency difference diagrams, observation minus model, scaled by the mode mass Q_{nl}, for the standard solar model (ssm), the turbulent pressure solar model (psm), a solar model with fixed turbulent pressure and kinetic energy (esm1), and a solar model with evolutionary turbulent pressure and kinetic energy (esm2, almost overlaps with esm1). Plotted are the $l = 0, 1, 2, 3, 4, 10, 20, \ldots, 100$ *p*-modes.

10.3 Solar model with turbulent pressure alone

The simplest way to take into account turbulence in solar modeling is to include turbulent pressure (or Reynolds stress) alone. In this case, only the hydrostatic equilibrium equation needs to be modified as follows:

$$\frac{\partial P}{\partial M_r} = -\frac{GM_r}{4\pi r^4}(1+\beta), \tag{32}$$

where $P = P_{\text{gas}} + P_{\text{rad}}$, and

$$\beta = \left(\frac{2P_{\text{turb}}}{\rho g r} - \frac{\partial P_{\text{turb}}}{\partial P}\right)\left(1 + \frac{\partial P_{\text{turb}}}{\partial P}\right)^{-1}. \tag{33}$$

Here $2P_{\text{turb}}/(\rho g r)$ originates from the spherical coordinate system adopted, representing a kind of geometric effect. The equations that govern the envelope integrations also need to be changed accordingly.

One can construct a calibrated nonstandard model in the same way as one obtains the standard solar model, assuming that P_{turb}, set equal to its value for the present sun, does not change from the ZAMS to the present age of the sun. The *p*-mode oscillation spectrum of this calibrated solar model (psm) is discussed in Sect. 10.5.

10.4 Solar model with χ and γ as independent variables

The form of the continuity equation and of the equation of transport of energy by radiation are not affected by turbulence. The hydrostatic equation includes a Reynolds stress term due to turbulence

$$\frac{\partial P}{\partial r} = -\frac{GM_r}{r^2}\rho - \frac{1}{r^2}\frac{d}{dr}(r^2\rho v_r v_r), \tag{34}$$

where $P = P_{\text{gas}} + P_{\text{rad}}$. Since the last term can be rewritten as $\partial P_{\text{turb}}/\partial r + 2(\gamma-1)\chi/r$, this equation becomes

$$\frac{\partial P_T}{\partial M_r} = -\frac{GM_r}{4\pi r^4} - \frac{2(\gamma-1)\chi}{4\pi r^3}. \tag{35}$$

The last term on the right hand side of Eq. (35) also embodies the same spheric geometric effect as $2P_{\text{turb}}/(\rho g r)$ in Eq. (33).

The energy conservation equation is also modified by turbulence because the first law of thermodynamics must now include the turbulent kinetic energy. We have then:

$$\frac{\partial L_r}{\partial M_r} = \varepsilon - T\frac{dS_T}{dt}, \tag{36}$$

where

$$T dS_T = c_p dT - \frac{\mu'}{\rho}dP_T + \left(1 + \frac{P_T\mu'\nu}{\rho\mu\chi}\right)d\chi + \frac{P_T\mu'\nu'}{\rho\mu\gamma}d\gamma. \tag{37}$$

The equation of energy transport by convection,

$$\frac{\partial T}{\partial M_r} = -\frac{T}{P_T}\frac{GM_r}{4\pi r^4}\nabla_{\text{conv}}, \tag{38}$$

does not change in form, but the convective temperature gradient, discussed in a previous section, is different from that without turbulence. The equations that govern envelope integrations also need to be changed accordingly. The oscillation properties of the calibrated solar model constructed under this assumption (esm) are discussed in the next section.

10.5 Frequency corrections to solar *p*-modes

Implementing the effects of turbulence in the outer layers of the stellar model modifies the calculated *p*-mode frequencies at high frequencies. The magnitude of the frequency

correction is illustrated in Fig. 1 and Fig. 2 for the case of a solar model, taken from the work of Li et al. (2002). In the Li et al. (2002) paper, the *p*-mode frequencies for two calibrated solar models that include the effects of turbulence are compared to the standard solar model (ssm) *p*-mode frequencies. The psm model is obtained by including turbulent pressure alone in the solar modeling, while the esm models are obtained by introducing the turbulent variables χ and γ which include both turbulent pressure and kinetic energy. Contrary to a frequently made assertion, the inclusion of turbulent pressure in the pressure term has only a small effect on the calculated *p*-mode frequencies. On the other hand, the inclusion of turbulent kinetic energy is significant. This is illustrated in Fig. 1 which shows that the frequency differences caused by turbulent kinetic energy are much larger in size than those caused by turbulent pressure alone. Fig. 2 indicates that the frequency changes caused by turbulent kinetic energy make the computed model frequencies match the solar data better than the ssm model. This result is consistent with the work of Rosenthal et al. (1999) who "patched" a modified 3D RHD simulation by Stein & Nordlund (1989) onto a 1D solar model (see their Figures 1 and 6).

10.6 SAL peak shift

While it is always preferable to extract the γ-χ data from a 3D RHD simulation that corresponds to exactly the same atmospheric conditions (log g, log T_{eff}) as in the 1D model, it is of interest to estimate the turbulence effects in stellar models where the 3D RHD simulation is not available.

In such situations, the γ-χ data cannot be used directly, instead the data must be shifted in order to be applied at the correct depth of the model (Straka et al. 2006). This shifting is motivated by an expected characteristic found in all 3D RHD atmosphere simulations: namely that the SAL peak closely coincides with the turbulent pressure peak.

10.7 Calibration

The presented method for including turbulence does not remove MLT and therefore the uncertainties inherent in the mixing length parameter remain. In order to make quantitative predictions, both mass and age of the star must be known to high precision in addition to the luminosity L and effective temperature T_{eff}. Instead of the latter an interferometric radius measurement is preferable, since the measurement is usually more precise.

In the case of the Sun, the age is known to high precision and the mixing length parameter and hydrogen mass fraction can be calibrated to the known solar luminosity and radius. As demonstrated in Guenther et al. (2005); Straka et al. (2006), asteroseismic data can be instrumental in other stars, since low order *p*-mode frequencies anchor the interior model effectively in age and mass. When calibrated to the same luminosity and effective temperature, a differential assessment of turbulence effects can be derived.

Another example, in which a proper calibration is possible with more asteroseismic data, is the detached binary system α Centauri: The masses of both components are known to high precision, the radius of the *A* component is measured with interferometric techniques (Kervella et al. 2003) and the luminosity is also well determined through parallax measurements. With the help of future asteroseismic data of the low order *p*-mode frequency spectrum, the stellar age of α Centauri can be effectively determined. Under such circumstances the methods described to include turbulence in YREC are fully applicable.

11 Seismic diagnostics

Stellar models constructed with YREC have been used to develop seismic diagnostics to explore internal structural properties of stars that could not be observed by any other means.

Basu et al. (2004) have used low degree acoustic modes to determine the *helium abundance* in the envelopes of low-mass main sequence stars with precision. The oscillatory signal in the frequencies caused by the depression in Γ_1 in the second helium ionization zone is used. For frequency errors of one part in 10^4, the expected σ_Y in the estimated Y ranges from 0.03 for $0.8 M_\odot$ stars to 0.01 for $1.2 M_\odot$ main sequence stars. In more evolved stars, this approach is feasible if the relative errors in the frequencies are less than 10^{-4}.

Mazumdar et al. (2006) have explored asteroseismic diagnostics of *convective core mass* using small frequency separations of low-degree *p*-modes. Small separations can also be combined to derive convective *core overshoot* diagnostics. It was shown that in stars with convective cores, the mass of the convective core can be estimated to within 5% if the total mass is known, although systematic errors in the total mass could introduce errors of up to 20%. The evolutionary stage of the star, determined in terms of the central hydrogen content is much less sensitive to the mass estimate.

12 Solar neutrinos and helioseismology

Different versions of YREC have been used to study the structure of the solar interior, the solar neutrino problem and helioseismology (Guenther & Demarque 1997) and references therein. In particular, the important series of papers by Bahcall et al. (2004, 2005) on solar neutrinos, helioseismology and solar abundances also made use of a dedicated version of YREC.

13 Other YREC applications

A variety of applications to stellar structure theory and evolution have been carried out using YREC. In addition of the work on stellar rotation mentioned in the introduction (see also Chaboyer et al. (1995) and Barnes (2003)), one notes

the pioneer work on stellar collisions and mergers (Sills et al. 1997).

Important research in stellar population studies and population synthesis continues to be carried out with the Yonsei-Yale isochrones (YY isochrones) (Yi et al. 2001). Frequently quoted research on helium burning phases of evolution (horizontal-branch) has also been carried out with YREC (Lee et al. 1994; Yi et al. 1997).

References

Angulo, C., Arnould, M., Rayet, M., et al. 1999, Nuclear Physics A, 656, 3

Bahcall, J. N. 1989, Neutrino astrophysics. (Cambridge University Press, Cambridge and New York, 1989, p. 584)

Bahcall, J. N., Basu, S., Pinsonneault, M., & Serenelli, A. M. 2005, ApJ, 618, 1049

Bahcall, J. N., Serenelli, A. M., & Pinsonneault, M. 2004, ApJ, 614, 464

Bahcall, J. N. & Ulrich, R. K. 1988, Reviews of Modern Physics, 60, 297

Barnes, S. A. 2003, ApJ, 586, 464

Basu, S., Mazumdar, A., Antia, H. M., & Demarque, P. 2004, MNRAS, 350, 277

Böhm-Vitense, E. 1958, Zeitschrift für Astrophysik, 46, 108

Canuto, V. M. & Mazzitelli, I. 1992, ApJ, 389, 724

Chaboyer, B., Demarque, P., & Pinsonneault, M. H. 1995, ApJ, 441, 865

Cox, J. P. & Giuli, R. T. 1968, Principles of stellar structure. (Gordon and Breach, New York, 1968)

Deliyannis, C. P. 1990, Ph.D. Thesis, Yale University

Edmonds, P., Cram, L., Demarque, P., Guenther, D. B., & Pinsonneault, M. H. 1992, ApJ, 394, 313

Endal, A. S. & Sofia, S. 1981, ApJ, 243, 625

Ferguson, J. W., Alexander, D. R., Allard, F., et al. 2005, ApJ, 623, 585

Guenther, D. B. 1994, ApJ, 422, 400

Guenther, D. B. & Brown, K. I. T. 2004, ApJ, 600, 419

Guenther, D. B. & Demarque, P. 1997, ApJ, 484, 937

Guenther, D. B., Kallinger, T., Reegen, P., et al. 2005, ApJ, 635, 547

Henyey, L. G., Wilets, L., Böhm, K. H., Lelevier, R., & Levee, R. D. 1959, ApJ, 129, 628

Iglesias, C. A. & Rogers, F. J. 1996, ApJ, 464, 943

Itoh, N., Adachi, T., Nakagawa, M., Kohyama, Y., & Munakata, H. 1989, ApJ, 339, 354

Kervella, P., Thévenin, F., Ségransan, D., et al. 2003, A&A, 404, 1087

Kim, Y.-C. & Chan, K. L. 1998, ApJL, 496, 121

Kippenhahn, R. & Thomas, H.-C. 1970, in Proc. IAU Colloq. 4, ed. A. Slettebak, 20

Kippenhahn, R. & Weigert, A. 1990, Stellar Structure and Evolution. (Springer-Verlag, Berlin, 1990)

Krishna Swamy, K. S. 1966, ApJ, 145, 174

Kuhfuß, R. 1986, A&A, 160, 116

Kurucz, R. L. 1998, http://kurucz.harvard.edu/grids.html

Larson, R. B. & Demarque, P. R. 1964, ApJ, 140, 524

Law, W. Y. 1980, Ph.D. Thesis, Yale University

Lee, Y.-W., Demarque, P., & Zinn, R. 1994, ApJ, 423, 248

Li, L. H., Robinson, F. J., Demarque, P., Sofia, S., & Guenther, D. B. 2002, ApJ, 567, 1192

Li, L. H., Ventura, P., Basu, S., Sofia, S., & Demarque, P. 2006, ApJS, 164, 215

Lydon, T. J., Guenther, D. B., & Sofia, S. 1996, ApJL, 456, L127

Lydon, T. J. & Sofia, S. 1995, ApJS, 101, 357

Mazumdar, A., Basu, S., Collier, B. L., & Demarque, P. 2006, MNRAS, 372, 949

Pinsonneault, M. H. 1988, Ph.D. Thesis, Yale University

Prather, M. J. 1976, Ph.D. Thesis, Yale University

Robinson, F. J., Demarque, P., Li, L. H., et al. 2003, MNRAS, 340, 923

Robinson, F. J., Demarque, P., Li, L. H., et al. 2004, MNRAS, 347, 1208

Rogers, F. J. & Nayfonov, A. 2002, ApJ, 576, 1064

Rosenthal, C. S., Christensen-Dalsgaard, J., Nordlund, Å., Stein, R. F., & Trampedach, R. 1999, A&A, 351, 689

Schwarzschild, M. 1958, Structure and evolution of the stars. (Princeton, Princeton University Press, 1958)

Sills, A., Lombardi, Jr., J. C., Bailyn, C. D., et al. 1997, ApJ, 487, 290

Stein, R. F. & Nordlund, A. 1989, ApJL, 342, L95

Stothers, R. B. & Chin, C.-W. 1995, ApJ, 440, 297

Straka, C. W., Demarque, P., & Guenther, D. B. 2005, ApJ, 629, 1075

Straka, C. W., Demarque, P., Guenther, D. B., Li, L., & Robinson, F. J. 2006, ApJ, 636, 1078

Thoul, A. A., Bahcall, J. N., & Loeb, A. 1994, ApJ, 421, 828

Unno, W. & Spiegel, E. A. 1966, PASJ, 18, 85

Wuchterl, G. & Feuchtinger, M. U. 1998, A&A, 340, 419

Yi, S., Demarque, P., & Kim, Y.-C. 1997, ApJ, 482, 677

Yi, S., Demarque, P., Kim, Y.-C., et al. 2001, ApJS, 136, 417

Zahn, J.-P. 1991, A&A, 252, 179